Calculating α-decay half-lives with artificial neural networks considering the effects of angular momentum and deformation

Hong-Qiang You,[1,2] Ren-Hang Wu,[1] Hao-Ze Su,[1] Jing-Jing Li,[1] Hai-Qian Zhang ●,[1] and Xiao-Tao He ●[1,*]

[1]*Nanjing University of Aeronautics and Astronautics*, Nanjing 210016, China
[2]*Clinical Oncology School of Fujian Medical University, Fujian Cancer Hospital*, Fuzhou, Fujian 350014, China

Artificial neural networks (ANNs) can be used to learn complex representations of data, enabling new approaches to modeling and processing in the physical sciences. In this work, ANNs are employed to calculate the α-decay half-lives of nuclei. An improvement in the predictive power of the ANN models can be achieved by incorporating the angular momentum transferred by α particle and the quadrupole deformation of parent nuclei. Consequently, the root-mean-square deviation between the ANN-predicted α-decay half-lives and the experimental data is reduced from 0.581 to 0.334. Predictions are made for the α-decay half-lives of isotopes with $Z = 117$, 118, 119, and 120. Based on the characteristics (or systematics) of the α-decay half-lives, we propose that $N = 184$ is a closed neutron shell beyond $N = 126$.

I. INTRODUCTION

In 1899, Rutherford discovered α-decay phenomenon. Gamow and Condon later demonstrated in 1928 that the α-decay process is due to quantum tunneling [1,2]. Since then, α decay has been acknowledged as a crucial method for examining unstable nuclei and gaining significant information about their structure. Many theoretical methods have been developed to study the nuclear α-decay half-life, including both of phenomenological and microscopic models, such as the generalized liquid drop model (GLDM) [3–5], the Coulomb and proximity potential model (CPPM) [6], the two-potential approach (TPA) [7,8], the unified fission model (UFM) [9], and the density-dependent cluster model (DDCM) [10]. In addition, many empirical formulas are used to calculate the α-decay half-lives, such as the Viola-Seaborg formula [11], the improved Geiger-Nuttall law (GN) [12], the Brown formula [13], the Royer's formula [3], the universal decay law (UDL) [14], and so on.

Recently, machine learning (ML) has been applied in nuclear physics [15,16]. This includes theoretical applications such as nuclear structure, nuclear reactions, and properties of nuclear matter, as well as experimental applications such as event identification and reconstruction, complex system control, and firmware performance. In nuclear structure, it includes research of estimating β-decay half-life [17], studying nuclear charge radii [18–20], predicting the α-decay energy of superheavy nuclei, and determining binding energies and two-nucleon separation energies of nuclei [21–26]. In the field of nuclear reactions, machine learning is a valuable tool for developing predictive models to describe and analyze nuclear reaction data. This includes refining the description of reaction

data [27], investigating the initial states of nuclei and reaction geometries [28], as well as exploring reaction mechanisms and phase transitions [29,30]. In addition, machine learning benefits nuclear experiments and the research of properties of dense matter in many ways [31–37].

The deep learning method is used to investigate α-decay half-lives [38,39]. In Ref. [38], α-decay half-lives are calculated for nuclei in the range $82 \leqslant Z \leqslant 118$ from four different ML models. These models include the XGBoost, the random forest (RF), the decision trees (DTs), and the multilayer perception (MLP) neural network. It turns out that XGBoost performs best, with the root-mean-square deviation of 0.646. In Ref. [39], word vectors, which are high-dimensional representations of nuclei from the hidden layers of the mass-regression deep neural network (DNN), are used to calculate α-decay half-lives. This method uses deviations of experimental values from those calculated by the theoretical model as targets rather than the direct experimental values to calculate the α-decay half-lives. The deviation of experimental values from the calculated results by the three-parameter Gamow formula [40] on 159 even-even nuclei is reduced from 0.3627 to 0.2297 on the α-decay half-lives.

In this work, artificial neural networks (ANNs) are constructed to study α-decay half-lives of nuclei. In addition to two quantities related to the pairing and shell effects, other physical features are incorporated into the inputs. Two quantities related to the effects of angular momentum and deformation of the parent nuclei are considered. Their influences on the predictive performance of ANN model are investigated. Finally, the ANN models with different inputs are applied to predict α-decay half-lives of the superheavy nuclei with $Z = 117$, 118, 119, and 120.

This paper is organized as follows. In Sec. II, the network structure of ANN model, input data and hyperparameters of the network are presented. In Sec. III, the results of α-decay
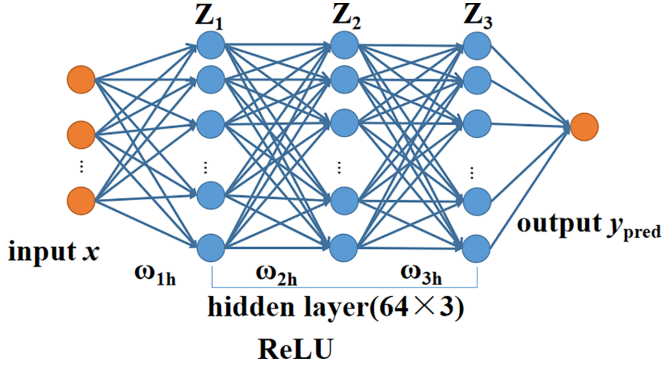
FIG. 1. The architecture of a typical fully connected feed-forward network with an input layer of specified units, three hidden layers of 64 units each, and a single output unit.

half-life calculations are presented using the ANN models, discussing the impact of angular momentum transferred by the α particle and the quadrupole deformation β_2 of the parent nuclei on these half-lives. The α-decay half-lives of even-even and odd-A nuclei with $Z = 117, 118, 119$, and 120 are predicted. A brief summary is given in Sec. IV.

II. THEORETICAL FRAMEWORK

Our model takes some quantities related to physical features as inputs, and the corresponding α-decay half-lives of nuclei as output. A ML model is assumed as below:

$$y_{\omega,b}(\boldsymbol{x}) = \phi(\boldsymbol{x}, \boldsymbol{\omega}), \tag{1}$$

where ϕ is the activation function. $\boldsymbol{\omega} = \{\omega_i\}$ are the weight parameters and $\boldsymbol{x} = \{x_i\}$ are the input data. In the context of ML, the parameters ω_i are optimized by minimizing loss function. In this manner, it is possible to make predictions that are as close as possible to the experimental data.

Multilayer perception (MLP) [41], which belongs to a class of feed-forward artificial neural networks, is chosen as the model to solve regression problems. MLP contains three layers called input layer, hidden layer (s), and output layer. In backpropagation based on error optimization, weights of hidden layers are adjusted iteratively.

As shown in Fig. 1, the data flow in the feed-forward neural network is given by the following equation for the adjacent layer:

$$z_i = \mathrm{ReLU}\left(\omega_{ih}^T x\right)$$

$$= \mathrm{ReLU}\left(\sum_{j=1}^{d} \omega_{ihj} x_j\right), h = 1, \dots, H_i, i = 1, 2, 3, \tag{2}$$

where z_i represents the value of the ith neuron in the next layer, and x_j represents the value of the jth neuron in the previous layer. ω_{ih} are the weight parameters belonging to the ith layer. The rectified linear unit (ReLU) function is chosen as the activation function with $\mathrm{ReLU}(x) = \log[1 + \exp(x)]$. While input x is entered into the input layer, it is first linearly transformed through $Z_i = x_j \omega_{ij}$ and then passed to a nonlinear activation ReLU. The output y_{pred} is result of the output layer.

To ensure homogeneity between the training set and the testing set, the sample of α-decay half-lives experimental data is sorted based on α-decay energy. The input data are divided into two subsets: 80% for training and 20% for testing. A pragmatic goal of the training process will be to minimize the error of mean square with respect to the experimental data. For the available experimental data $D = \{(x_1, y_1), (x_2, y_2), \cdots, (x_n, y_n)\}$, where x_i and y_i $(i = 1, 2, \dots, n)$ are input and output data and n is the number of data, the loss function is given as:

$$E(\boldsymbol{\omega}, \boldsymbol{v}|D) = \sum_{t=1}^{n} (e_t)^2 = \frac{\sum_{t=1}^{n} \left(y_t^{\mathrm{pred}} - y_t^{\mathrm{exp}}\right)^2}{n}. \tag{3}$$

Here y_t^{pred} $(t = 1, 2, \dots, n)$ is the output of the ANN model, whereas y_t^{exp} $(t = 1, 2, \dots, n)$ is the experimental α-decay half-life $\log_{10} T_{1/2}$. e_t is the deviation of experimental value from the output of ANN model.

The ANN model is built in PYTHON. Keras and Adam optimization algorithm is used to train our ANN model for 1000 epochs to minimize the loss function. The hyperparameter called the regularizer is used to avoid overfitting. The callbacks are applied to monitor the loss function to find a smaller value of the loss function.

III. RESULTS AND DISCUSSIONS

A. Effect of pairing and shell closure on α-decay half-lives with ANN models

In nuclear physics, apart from the mass number A and the proton number Z, the pairing and shell effects (δ, P) [42–44] are widely used to improve the performance of the ANN model [45,46]. In this work, the pairing and shell effects (δ, P) are also taken as inputs to test the performance of ANN model for the calculation of α-decay half-lives. The corresponding magic numbers are taken to be 8, 20, 28, 50, 82, 126, and 184. The experimental α-decay half-lives, spin, and parity are taken from the evaluated nuclear properties table NUBASE2016 [47]. The α-decay energy are taken from the evaluated atomic mass table AME2016 [48,49]. A total of 606 α-decay half-lives of nuclei are extracted. To quantity the performance of the ANN model in describing α-decay half-lives for both the training and testing sets, the root-mean-square (σ_{RMS}) deviations are utilized and defined as follows:

$$\sigma_{\mathrm{RMS}} = \sqrt{\sum_{i=1}^{n} \left[\log_{10}\left(T_{1/2}^{\mathrm{cal}} / T_{1/2}^{\mathrm{exp}}\right)_i\right]^2 / \mathrm{n}}, \tag{4}$$

where $T_{1/2}^{\mathrm{cal}}$ are the predictions from the ANN model and $T_{1/2}^{\mathrm{exp}}$ are the experimental α-decay half-lives.

Table I shows the σ_{RMS} deviations of α-decay half-lives of the ANN models with respect to the experimental data in different data sets. It is found that by incorporating pairing effect δ into the ANN2 model, the value of σ_{RMS} for the entire set is reduced by 14.4%, from 0.692 in the ANN1 model to 0.599 in the ANN2 model. Similarly, when shell effect P is incorporated into the ANN3 model, the value of σ_{RMS} for the entire set is reduced by only 4.3%, from 0.692 in the ANN1

TABLE I. The σ_{RMS} for the training set (484 nuclei) and testing set (122 nuclei) with different ANN models.

	Inputs	σ_{RMS} (Testing set)	σ_{RMS} (Training set)	σ_{RMS} (Entire set)
ANN1	$A_p, Z_p, A_d, Z_d, Q_\alpha$	0.752	0.677	0.692
ANN2	$A_p, Z_p, A_d, Z_d, \delta, Q_\alpha$	0.745	0.556	0.599
ANN3	$A_p, Z_p, A_d, Z_d, P, Q_\alpha$	0.750	0.610	0.670
ANN4	$A_p, Z_p, A_d, Z_d, \delta, P, Q_\alpha$	0.684	0.552	0.581
ANN5	$A_p, Z_p, A_d, Z_d, l, Q_\alpha$	0.545	0.377	0.416
ANN6	$A_p, Z_p, A_d, Z_d, l, \delta, Q_\alpha$	0.542	0.370	0.404
ANN7	$A_p, Z_p, A_d, Z_d, l, P, Q_\alpha$	0.497	0.368	0.399
ANN8	$A_p, Z_p, A_d, Z_d, l, \delta, P, Q_\alpha$	0.385	0.295	0.335
ANN9	$A_p, Z_p, A_d, Z_d, l, \beta_2, Q_\alpha$	0.477	0.368	0.398
ANN10	$A_p, Z_p, A_d, Z_d, l, \delta, \beta_2, Q_\alpha$	0.425	0.300	0.350
ANN11	$A_p, Z_p, A_d, Z_d, l, P, \beta_2, Q_\alpha$	0.476	0.365	0.396
ANN12	$A_p, Z_p, A_d, Z_d, l, \delta, P, \beta_2, Q_\alpha$	0.385	0.293	0.334

model to 0.670 in the ANN3 model. Additionally, pairing and shell effects are simultaneously incorporated into the ANN4 model. The value of σ_{RMS} for the entire set decreases from 0.692 in the ANN1 model to 0.581 in the ANN4 model, which is a decrease of 16.1%. Such accuracy is insufficient for the investigation of α-decay half-lives. This indicates that adding two additional inputs (δ and P) does not significantly enhance the predictive power of the ANN model. Therefore, more physical features are incorporated into the input layer, i.e., we will include two quantities related to the effects of angular momentum and deformation. Their influences on predictive performance of the ANN model are investigated.

B. Effect of angular momentum on α-decay half-lives with ANN models

Previous studies have shown that the angular momentum l taken away by α particle can affect the calculation of α-decay half-lives through the centrifugal potential [50,51]. In this work, the angular momentum is taken into account by introducing the input l, which is determined by [52]:

$$l = \begin{cases} \Delta_j, & \text{for even } \Delta_j & \text{and} & \pi_p = \pi_d, \\ \Delta_j + 1, & \text{for even } \Delta_j & \text{and} & \pi_p \neq \pi_d, \\ \Delta_j, & \text{for odd } \Delta_j & \text{and} & \pi_p \neq \pi_d, \\ \Delta_j + 1, & \text{for odd } \Delta_j & \text{and} & \pi_p = \pi_d, \end{cases} \quad (5)$$

where $\Delta_j = |j_d - j_p|$, j_d, π_d (j_p, π_p) are the spin and parity values of the daughter (parent) nucleus, respectively.

The σ_{RMS} deviations for different ANN models are given in Table I. By incorporating the angular momentum l into the ANN5 model, the σ_{RMS} reduces from 0.752 to 0.545 for the testing set and from 0.677 to 0.377 for the training set compared to the ANN1 model. For the entire set, σ_{RMS} of the ANN5 model is reduced by 40% compared to the ANN1 model. This demonstrates that including the angular momentum effect as an input improves the predictive power of the ANN model. Similarly, the angular momentum is taken into consideration in the ANN6, ANN7, and ANN8 models. It is found that σ_{RMS} values for the entire set in the ANN6, ANN7, and ANN8 models are reduced by 32.5%, 40.4%, and 42.3% compared to the values in the ANN2, ANN3, and ANN4 models, respectively. It further shows that the consideration

of angular momentum can improve prediction accuracy of the ANN model.

The σ_{RMS} deviations provide only a gross assessment of the accuracy of ANN models. To provide a more detailed view, the differences between the experimental α-decay half-lives and the predictions from various ANN models are illustrated in Fig. 2. It can be seen that the ANN1 model performs relatively poorly. Nuclei with deviations greater than 0.6 from the experimental values are predominantly found in the region where $N > 126$, as shown in Fig. 2(a). The above discussion suggests that the effects of pairing and shell closure cannot obviously improve the calculated results. This phenomenon is more pronounced around the magic numbers ($N = 126$ and $Z = 82$) as shown in Fig. 2(b). The discrepancies between the experimental data and the predictions from different ANN models are generally attributed to missing physics. By incorporating quantities related to the effect of angular momentum as inputs, the ANN model is expected to better capture this missing physics. By taking the angular momentum as the input, the deviations from the experimental values are evidently reduced as shown in Fig. 2(c), especially for the nuclei around magic number region. Compared to Fig. 2(a), it is evident that incorporating angular momentum l enhances the accuracy of the ANN model more effectively than pairing and shell effects (δ and P). Compared to Fig. 2(c), Fig. 2(d) shows that calculated results from the ANN8 model align more closely with the experimental data, both for the nuclei near magic number regions and for those in other regions. It suggests that a better description can be achieved by considering the effect of angular momentum in the ANN models.

Figures 3 and 4 show the values of σ_{RMS} deviations between calculated results from the ANN models and the experimental data for the nuclei with different angular momentum l values. Except for $l = 4$, larger values of angular momentum l taken by the α particle correspond to higher σ_{RMS} values for the ANN1 and ANN4 models, which do not account for the effect of angular momentum. For $l = 4$, there are only six experimental data, which is about 1% of the total sample data. Therefore, the ANN models cannot learn this performance. When $l = 5$, the σ_{RMS} between calculated and experimental values is the largest, with a value greater than 1. As shown in Figs. 3 and 4, when considering the effect
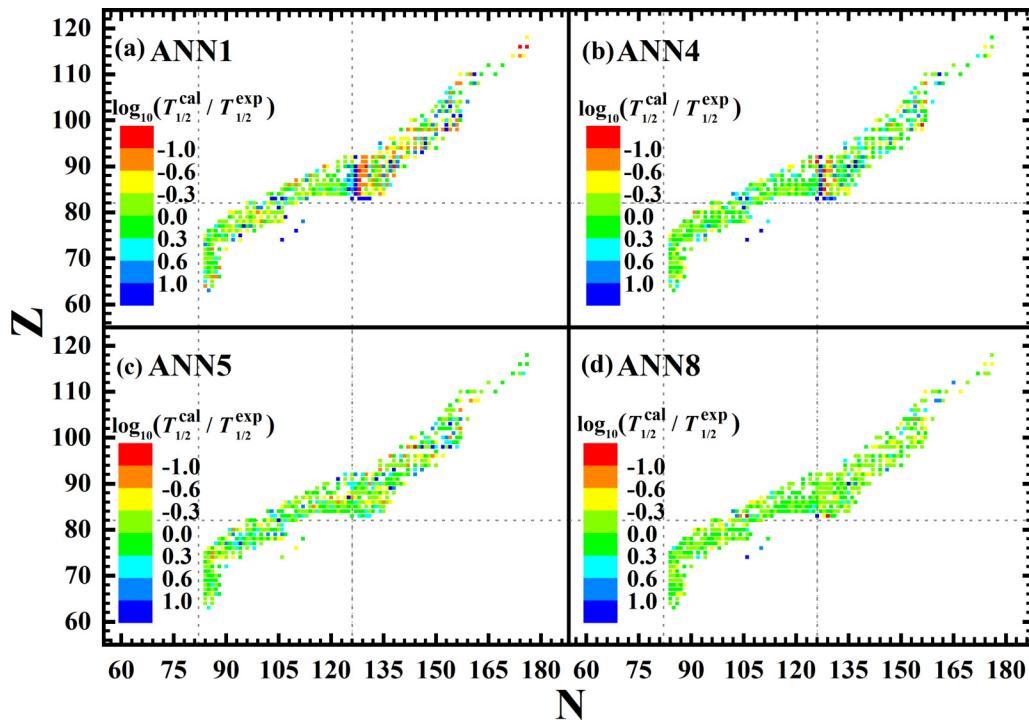
FIG. 2. Logarithmic differences between experimental α-decay half-lives and calculated results obtained by the ANN1, ANN4, ANN5, and ANN8 models. The dashed lines represent the neutron magic numbers $N = 82$, 126 and the proton magic number $Z = 82$.

of angular momentum on the nuclei with different angular momentum l, σ_{RMS} values of the ANN5 and ANN8 models decrease compared to those of the ANN1 and ANN4 models.

C. Effect of deformation of the parent nuclei on α-decay half-lives with ANN models

For many heavy isotopes, especially for superheavy nuclei, deformation plays an important role in radioactive decay [53,54]. In Refs. [55,56], it shows that α-decay width is sensitive to nuclear deformation. Therefore, an attempt is made to investigate the effect of quadrupole deformation β_2

of parent nuclei on the performance of ANN model. The quadrupole deformation parameters are taken from Ref. [57].

As shown in Table I, on the basis of the ANN5, ANN6, and ANN7 models, the quadrupole deformation β_2 of parent nuclei is incorporated into the ANN9, ANN10, and ANN11 models. The corresponding σ_{RMS} values for the entire set reduce from 0.416 to 0.398, 0.404 to 0.350, and 0.399 to 0.396, respectively. It shows that consideration of the quadrupole deformation β_2 of parent nuclei can improve the predictive power of ANN model. The σ_{RMS} value of the ANN10 model is 0.350, indicating that it can well reproduce the experimental
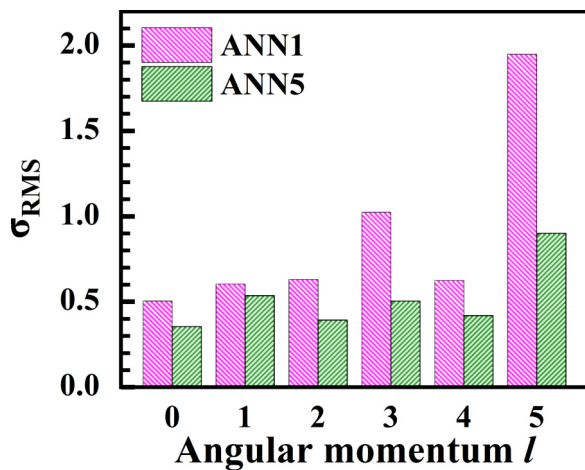

FIG. 3. Root-mean-square deviation σ_{RMS} of the ANN1 and ANN5 models for α-decay half-lives with different angular momentum l.
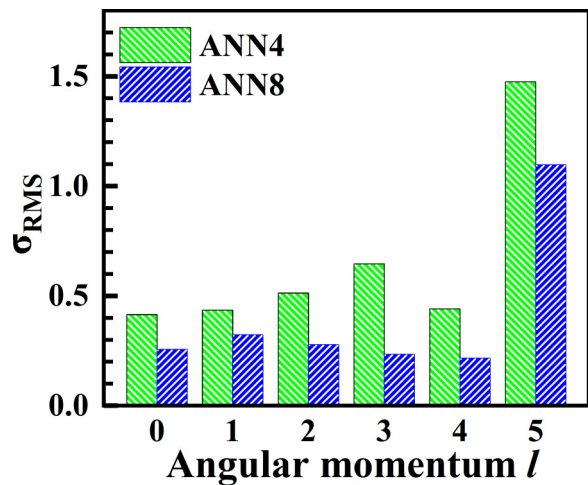

FIG. 4. Root-mean-square deviation σ_{RMS} of the ANN4 and ANN8 models for α-decay half-lives with different angular momentum l.
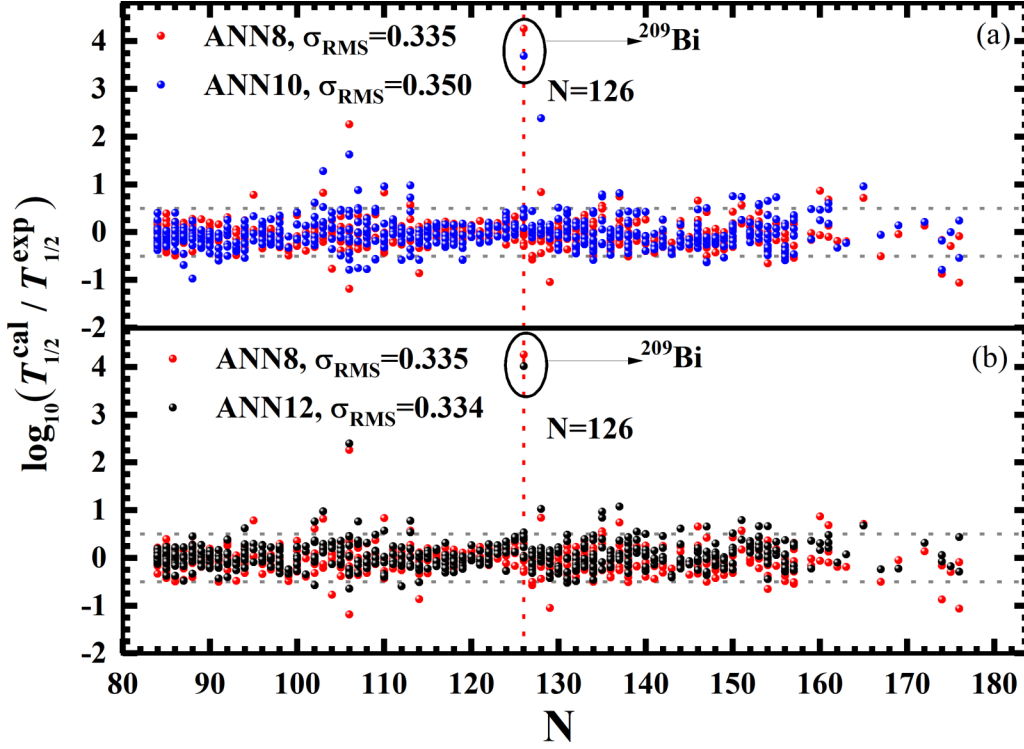
FIG. 5. Logarithmic differences between the experimental α-decay half-lives and the calculated results obtained from different ANN models. (a) shows the calculated results obtained from ANN8 and ANN10 models. (b) shows the calculated results obtained from ANN8 and ANN12 models. The gray dashed lines denote the logarithmic difference is within 0.5. The red dashed line represents the magic number $N = 126$.

α-decay half-lives. Moreover, taking quadrupole deformation of the parent nuclei as input can avoid the uncertainty associated with magic and submagic numbers, as well as provide early insights into shell structure. It offers a method for predicting magic and submagic numbers in the superheavy nuclear region. When both deformation and shell effects are considered, the ANN12 model performs the best for the entire set with a σ_{RMS} value of 0.334, demonstrating its ability to well reproduce the experimental α-decay half-lives.

In Fig. 5, it can be seen that the nuclei with large deviations from the experimental values are generally located in the same regions surrounded by black ovals. This indicates that some physical features are still missing in the ANN model and these features will affect the predictions of α-decay half-lives for some nuclei. It can be seen that the decimal logarithm of $T_{1/2}^{cal}/T_{1/2}^{exp}$ for ^{209}Bi is larger than 3 for different ANN models used in the present work, which is higher than the value of 1.5 obtained using the nuclear theoretical method in Ref. [50]. For ^{209}Bi, the angular momentum taken away by α particle is $l = 5$. There are only 19 such cases in the sample data, which constitute less than 3.5% of the total data. Lack of enough sample data for training should be one of main reasons for the large discrepancy between the predicted result and the experimental data for ^{209}Bi.

To better understand the performance of the ANN models with different inputs, results of the ANN models are compared with those of empirical formulas. The corresponding σ_{RMS} of the ANN models and empirical formulas are given in Table II. The σ_{RMS} of the ANN10 model for even-even nuclei is slightly

higher than that of the empirical formula [51]. However, the ANN8 and ANN10 models perform better overall than the empirical formulas. In particular, for odd-odd nuclei, the σ_{RMS} values for the ANN8 and ANN10 models decrease by 47.5% and 37.3%, respectively, compared to the values obtained from the empirical formula in Ref. [51]. Similarly, for all nuclei, σ_{RMS} of the ANN8 and ANN10 models are decreased by 34.2% and 29.7%, respectively, compared to the values from the empirical formula in Ref. [50].

It is worth noting that in standard α-decay theories, it is assumed that an α particle penetrates the deformed Coulomb barrier, which is only related to deformation of the daughter nucleus. Since in most cases, deformation value of the parent nucleus is close to that of daughter one, deformation of the parent nucleus is taken as one of inputs in present work for convenience. The results by taking quadrupole deformations

TABLE II. The σ_{RMS} between the experimental α-decay half-lives and the calculated results from ANN models and empirical formulas [50,51].

	ANN8	ANN10	Ref. [51]	Ref. [50]
e-e	0.303	0.353	0.319	0.371
e-o	0.264	0.314	0.496	0.462
o-e	0.437	0.445	0.472	0.426
o-o	0.282	0.337	0.538	0.481
All nuclei	0.335	0.350	0.433	0.432

TABLE III. Predicted α-decay half-lives of even-even nuclei and odd-A nuclei with $Z = 117$, 118, 119, and 120.

α transition	Q_α (MeV)	l	β_2 [57]	$\log_{10}T_{1/2}^{\mathrm{GLDM}}$ [50]	$\log_{10}T_{1/2}^{\mathrm{ANN8}}$	$\log_{10}T_{1/2}^{\mathrm{ANN10}}$	$\log_{10}T_{1/2}^{\mathrm{ANN12}}$
^{279}Ts $\rightarrow$ ^{275}Mc	13.49	2	0.08	−6.2	−5.837	−6.878	−5.774
^{281}Ts $\rightarrow$ ^{277}Mc	13.52	2	0.071	−6.3	−6.057	−6.779	−5.921
^{283}Ts $\rightarrow$ ^{279}Mc	13	2	0.071	−5.32	−5.131	−5.698	−5.275
^{285}Ts $\rightarrow$ ^{281}Mc	12.39	2	0.071	−4.07	−3.943	−4.257	−4.334
^{287}Ts $\rightarrow$ ^{283}Mc	11.92	2	0.08	−3.09	−2.853	−3.232	−3.573
^{289}Ts $\rightarrow$ ^{285}Mc	11.79	2	0.08	−2.81	−2.683	−2.972	−3.218
^{291}Ts $\rightarrow$ ^{287}Mc	11.46	2	0.072	−2.07	−1.979	−2.274	−2.306
^{293}Ts $\rightarrow$ ^{289}Mc	11.37	2	−0.087	−1.88	−1.928	−2.098	−2.058
^{295}Ts $\rightarrow$ ^{291}Mc	11.12	2	−0.07	−1.29	−1.450	−1.385	−1.346
^{297}Ts $\rightarrow$ ^{293}Mc	11.54	2	−0.008	−2.37	−2.691	−2.479	−2.394
^{299}Ts $\rightarrow$ ^{295}Mc	11.39	2	0	−2.04	−2.338	−2.184	−1.863
^{301}Ts $\rightarrow$ ^{297}Mc	11.54	2	0	−2.44	−2.780	−2.476	−2.085
^{303}Ts $\rightarrow$ ^{299}Mc	12.73	2	0	−5.13	−5.539	−5.164	−5.263
^{305}Ts $\rightarrow$ ^{301}Mc	12.13	2	0	−3.88	−4.449	−3.863	−3.981
^{307}Ts $\rightarrow$ ^{303}Mc	11	1	0	−1.4	−1.716	−1.511	−1.245
^{309}Ts $\rightarrow$ ^{305}Mc	10.01	3	−0.407	1.82	1.408	2.816	1.496
^{311}Ts $\rightarrow$ ^{307}Mc	8.84	2	0	5.27	4.903	6.932	5.769
^{313}Ts $\rightarrow$ ^{309}Mc	8.31	0	0.116	6.91	6.901	8.910	7.833
^{315}Ts $\rightarrow$ ^{311}Mc	8.91	5	0.331	6.17	5.684	7.248	6.733
^{317}Ts $\rightarrow$ ^{313}Mc	8.49	5	0.331	7.69	7.781	9.016	8.997
^{281}Og $\rightarrow$ ^{277}Lv	13.93	5	0.184	−5.43	−5.006	−6.199	−4.662
^{282}Og $\rightarrow$ ^{278}Lv	13.75	0	0.062	−7.02	−7.406	−7.793	−7.144
^{283}Og $\rightarrow$ ^{279}Lv	13.59	7	0.062	−3.51	−3.398	−4.582	−3.411
^{284}Og $\rightarrow$ ^{280}Lv	13.29	0	0.062	−6.17	−6.600	−6.736	−6.383
^{285}Og $\rightarrow$ ^{281}Lv	13.07	0	0.071	−5.41	−5.485	−6.357	−5.823
^{286}Og $\rightarrow$ ^{282}Lv	12.89	0	0.08	−5.43	−5.614	−5.893	−5.681
^{287}Og $\rightarrow$ ^{283}Lv	12.73	0	−0.104	−4.74	−4.743	−5.628	−5.761
^{288}Og $\rightarrow$ ^{284}Lv	12.52	0	0.08	−4.67	−4.690	−5.138	−5.079
^{289}Og $\rightarrow$ ^{285}Lv	12.44	0	0.08	−4.17	−4.139	−4.948	−4.883
^{290}Og $\rightarrow$ ^{286}Lv	12.41	0	−0.112	−4.49	−4.454	−4.928	−4.919
^{291}Og $\rightarrow$ ^{287}Lv	12.22	2	0.081	−3.4	−3.535	−3.707	−4.010
^{292}Og $\rightarrow$ ^{288}Lv	12.01	0	0.081	−3.64	−3.446	−4.109	−3.770
^{293}Og $\rightarrow$ ^{289}Lv	12.02	2	0.08	−2.99	−3.184	−3.306	−3.439
^{294}Og $\rightarrow$ ^{290}Lv	11.97	0	−0.087	−3.58	−3.393	−4.001	−3.539
^{295}Og $\rightarrow$ ^{291}Lv	11.7	0	−0.087	−2.6	−2.587	−2.703	−2.869
^{296}Og $\rightarrow$ ^{292}Lv	11.56	0	−0.079	−2.65	−2.355	−3.213	−2.349
^{297}Og $\rightarrow$ ^{293}Lv	12	0	−0.035	−3.33	−3.433	−3.467	−3.515
^{298}Og $\rightarrow$ ^{294}Lv	12.12	0	−0.008	−3.98	−3.890	−4.384	−3.646
^{299}Og $\rightarrow$ ^{295}Lv	11.99	2	−0.008	−3.05	−3.512	−3.247	−3.171
^{300}Og $\rightarrow$ ^{296}Lv	11.91	0	0	−3.53	−3.378	−3.905	−2.952
^{301}Og $\rightarrow$ ^{297}Lv	11.98	2	0	−3.05	−3.531	−3.233	−2.987
^{302}Og $\rightarrow$ ^{298}Lv	12	0	0	−3.77	−3.660	−4.136	−3.020
^{303}Og $\rightarrow$ ^{299}Lv	12.55	4	0	−3.62	−4.092	−3.583	−3.770
^{304}Og $\rightarrow$ ^{300}Lv	13.1	0	0	−6.17	−6.442	−6.390	−6.045
^{305}Og $\rightarrow$ ^{301}Lv	12.93	2	0	−5.17	−5.733	−5.313	−5.556
^{306}Og $\rightarrow$ ^{302}Lv	12.53	0	0	−5.02	−5.337	−5.259	−4.762
^{307}Og $\rightarrow$ ^{303}Lv	11.99	2	0.001	−3.17	−3.913	−3.310	−3.357
^{308}Og $\rightarrow$ ^{304}Lv	11.2	0	0.001	−1.97	−1.936	−2.470	−1.514
^{309}Og $\rightarrow$ ^{305}Lv	10.67	2	0.002	0.07	−0.361	0.576	0.059
^{310}Og $\rightarrow$ ^{306}Lv	10.29	0	0	0.45	0.638	0.527	0.661
^{311}Og $\rightarrow$ ^{307}Lv	9.39	2	0.003	3.86	3.574	5.247	4.171
^{312}Og $\rightarrow$ ^{308}Lv	9.06	0	0.003	4.29	4.249	5.014	4.477
^{313}Og $\rightarrow$ ^{309}Lv	8.76	0	0.541	5.7	5.763	7.572	6.779
^{314}Og $\rightarrow$ ^{310}Lv	8.5	0	0.542	6.29	5.940	7.217	6.650
^{315}Og $\rightarrow$ ^{311}Lv	8.4	3	0.543	7.66	7.957	9.661	9.375
^{316}Og $\rightarrow$ ^{312}Lv	8.47	0	0.34	6.4	6.052	7.320	6.511
^{317}Og $\rightarrow$ ^{313}Lv	8.09	3	0.331	8.84	9.688	10.483	10.818

TABLE III. (*Continued.*)

α transition	Q_α (MeV)	l	β_2 [57]	$\log_{10}T_{1/2}^{\text{GLDM}}$ [50]	$\log_{10}T_{1/2}^{\text{ANN8}}$	$\log_{10}T_{1/2}^{\text{ANN10}}$	$\log_{10}T_{1/2}^{\text{ANN12}}$
^{318}Og $\rightarrow$ ^{314}Lv	8.48	0	0.331	6.3	6.063	7.264	6.489
^{285}119 $\rightarrow$ ^{281}Ts	13.65	2	0.08	−5.99	−5.939	−6.644	−6.058
^{287}119 $\rightarrow$ ^{283}Ts	13.28	2	−0.104	−5.33	−5.320	−5.788	−5.906
^{289}119 $\rightarrow$ ^{285}Ts	13.08	2	0.089	−4.95	−5.048	−5.401	−5.360
^{291}119 $\rightarrow$ ^{287}Ts	12.87	2	0.081	−4.56	−4.760	−4.957	−5.119
^{293}119 $\rightarrow$ ^{289}Ts	12.51	2	0.081	−3.84	−4.011	−4.104	−4.431
^{295}119 $\rightarrow$ ^{291}Ts	12.57	2	0.072	−4.01	−4.363	−4.301	−4.548
^{297}119 $\rightarrow$ ^{293}Ts	12.3	2	−0.079	−3.46	−3.831	−3.662	−3.820
^{299}119 $\rightarrow$ ^{295}Ts	12.73	2	−0.018	−4.41	−4.940	−4.633	−4.836
^{301}119 $\rightarrow$ ^{297}Ts	12.37	0	0	−4	−4.089	−4.476	−3.927
^{303}119 $\rightarrow$ ^{299}Ts	12.37	2	0	−3.71	−4.191	−3.840	−3.593
^{305}119 $\rightarrow$ ^{301}Ts	13.45	2	0	−5.98	−6.463	−6.363	−6.361
^{307}119 $\rightarrow$ ^{303}Ts	12.82	0	0	−5.05	−5.596	−5.706	−5.299
^{309}119 $\rightarrow$ ^{305}Ts	11.34	3	0.001	−1.09	−1.680	−0.949	−1.208
^{311}119 $\rightarrow$ ^{307}Ts	10.6	0	0.003	0.2	0.043	0.396	0.246
^{313}119 $\rightarrow$ ^{309}Ts	9.5	2	0.004	3.78	3.672	5.356	4.196
^{315}119 $\rightarrow$ ^{311}Ts	9.31	1	0.541	4.18	4.319	5.763	5.435
^{317}119 $\rightarrow$ ^{313}Ts	9.25	3	0.36	4.84	4.880	6.601	5.595
^{319}119 $\rightarrow$ ^{315}Ts	8.49	6	0.331	9.13	9.199	10.602	10.404
^{287}120 $\rightarrow$ ^{283}Og	13.92	4	−0.096	−5.44	−5.252	−6.205	−5.649
^{288}120 $\rightarrow$ ^{284}Og	13.75	0	−0.113	−6.53	−7.070	−7.239	−7.408
^{289}120 $\rightarrow$ ^{285}Og	13.68	0	−0.122	−6.05	−6.507	−7.148	−7.292
^{290}120 $\rightarrow$ ^{286}Og	13.63	0	−0.122	−6.34	−6.843	−7.008	−7.261
^{291}120 $\rightarrow$ ^{287}Og	13.41	2	−0.13	−5.25	−5.529	−5.878	−6.224
^{292}120 $\rightarrow$ ^{288}Og	13.31	0	−0.13	−5.75	−6.050	−6.352	−6.603
^{293}120 $\rightarrow$ ^{289}Og	13.24	2	0.089	−4.96	−5.324	−5.383	−5.683
^{294}120 $\rightarrow$ ^{290}Og	13.07	0	0.081	−5.31	−5.468	−5.908	−5.851
^{295}120 $\rightarrow$ ^{291}Og	13.1	2	0.081	−4.71	−5.184	−5.103	−5.578
^{296}120 $\rightarrow$ ^{292}Og	13.19	0	−0.096	−5.58	−5.839	−6.156	−6.049
^{297}120 $\rightarrow$ ^{293}Og	13.02	0	−0.087	−4.9	−5.299	−5.795	−5.650
^{298}120 $\rightarrow$ ^{294}Og	12.9	0	−0.079	−5.03	−5.120	−5.586	−5.168
^{299}120 $\rightarrow$ ^{295}Og	13.19	0	−0.035	−5.27	−5.800	−6.118	−5.948
^{300}120 $\rightarrow$ ^{296}Og	13.29	0	−0.008	−5.85	−6.204	−6.374	−6.029
^{301}120 $\rightarrow$ ^{297}Og	13.04	2	−0.008	−4.69	−5.304	−5.084	−5.245
^{302}120 $\rightarrow$ ^{298}Og	12.88	0	0	−5.05	−5.161	−5.563	−4.821
^{303}120 $\rightarrow$ ^{299}Og	12.8	2	0	−4.23	−4.829	−4.469	−4.469
^{304}120 $\rightarrow$ ^{300}Og	12.75	0	0	−4.81	−4.860	−5.314	−4.323
^{305}120 $\rightarrow$ ^{301}Og	13.27	2	0	−5.24	−5.807	−5.585	−5.626
^{306}120 $\rightarrow$ ^{302}Og	13.82	0	0	−6.99	−7.366	−7.458	−7.270
^{307}120 $\rightarrow$ ^{303}Og	13.58	4	0.001	−5.16	−5.720	−5.502	−5.744
^{308}120 $\rightarrow$ ^{304}Og	13.04	0	0.001	−5.49	−5.898	−5.910	−5.446
^{309}120 $\rightarrow$ ^{305}Og	12.17	0	0.002	−3.28	−3.540	−3.637	−3.400
^{310}120 $\rightarrow$ ^{306}Og	11.48	0	0.003	−2.01	−1.887	−2.712	−1.606
^{311}120 $\rightarrow$ ^{307}Og	11.1	2	0.004	−0.41	−0.720	−0.170	−0.428
^{312}120 $\rightarrow$ ^{308}Og	11.05	0	0.004	−0.97	−0.874	−1.326	−0.665
^{313}120 $\rightarrow$ ^{309}Og	10.92	2	0.005	0.03	−0.220	0.483	−0.025
^{314}120 $\rightarrow$ ^{310}Og	9.97	0	0.005	2.06	2.889	5.117	5.304
^{315}120 $\rightarrow$ ^{311}Og	10.15	0	0.531	1.87	2.482	4.693	4.760
^{316}120 $\rightarrow$ ^{312}Og	9.97	0	0.541	2.05	2.710	4.836	5.325
^{317}120 $\rightarrow$ ^{313}Og	9.96	3	0.542	3.01	2.712	4.356	6.582
^{318}120 $\rightarrow$ ^{314}Og	9.99	0	0.543	1.95	2.281	4.839	5.149

of the parent nucleus and the daughter nucleus as inputs are checked separately for one of ANN models. It is found that the results of the two predictions are quite similar.

The data (606 nuclei) in NUBASE2016 are used as the training set while the newly evaluated data (74 nuclei) in NUBASE2020 are used as the testing set to verify the extrapolation ability of ANN8, ANN10, and ANN12 models. The corresponding values of σ_{RMS} for the training set are 0.217, 0.219, and 0.212, while those for the testing set are 0.669, 0.694, and 0.634, respectively. Additionally, the
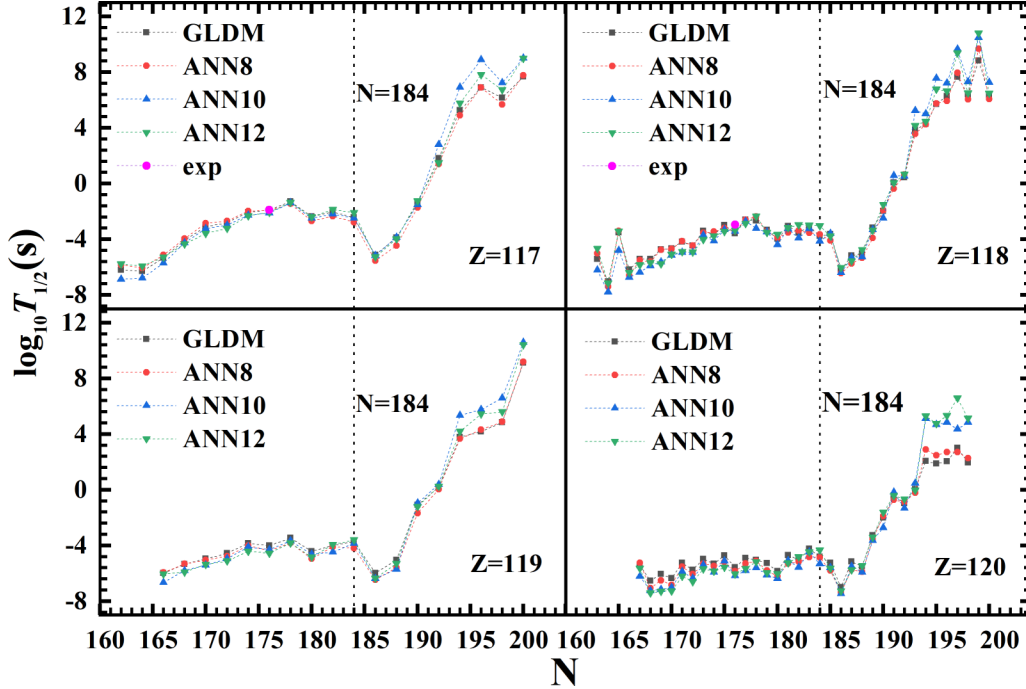
FIG. 6. Predicted logarithms of α-decay half-lives of nuclei with $Z = 117$, 118, 119, and 120 obtained by GLDM [50] and ANN models with different inputs. The black dashed lines denote the neutron number $N = 184$.

empirical formula proposed by Zhang *et al.* [50] is used to calculate α-decay half-lives of the newly evaluated nuclei in NUBASE2020. The value of σ_{RMS} deviation between calculated results by the empirical formula and the experimental data is 0.651.

D. α-decay half-lives in the superheavy nuclei mass region with ANN models

Accurate prediction of the decay properties of superheavy nuclei is very important for both of the synthesis and the structural study of superheavy elements [58,59]. As the above ANN models have been well trained, they are used to calculate the α-decay half-lives of nuclei in superheavy region. The α-decay half-lives of $Z = 117$, 118, 119, and 120 isotopes, calculated by the GLDM and ANN models, are listed in Table III. The first four columns represent the α decay, the decay energy Q_α, the angular momentum l taken away by α particle, and the quadrupole deformation parameter β_2 of parent nuclei, respectively. The logarithmic of α-decay half-lives calculated by the GLDM [50] and the ANN models 8, 10, 12 are listed in the fifth and sixth, seventh, eighth columns, respectively. The α-decay energy Q_α of superheavy nuclei has been determined from the WS3+ mass model [60], which has been shown to reproduce well the experimental Q_α of superheavy nuclei [61–63]. The spin and parity of these nuclei are taken from Ref. [64]. The quadrupole deformation parameter β_2 of parent nuclei is obtained by Ref. [57]. The logarithms of α-decay half-lives from the ANN and GLDM models are shown in Fig. 6. It can be seen that for ^{293}Ts and ^{294}Og, α-decay half-lives predicted by the ANN and GLDM models are in good agreement with the experimental data. The α-decay half-

lives of $Z = 117$, 118, 119, and 120 isotopes decrease sharply from $N = 184$ to $N = 186$. With only two more neutrons added, the α-decay half-lives decrease by over two orders of magnitude. This indicates that $N = 184$ could be the next neutron magic number after $N = 126$. Note that the shell structure is learned from the experimental data by the ANN10 model, like Q_α or deformation, since the shell effect P is not taken into account in it.

The deviations of α-decay half-lives of the nuclei with $Z = 117$, 118, 119, and 120 between the results from the ANN model and those from the GLDM model [50] are shown in Fig. 7. For isotopes with neutron numbers less than 194, the deviations between predictions from the ANN and the GLDM models are close to unity. It shows a good agreement between calculations of the ANN models and results of the GLDM model. The deviations become larger for the heavier isotopes with $N > 194$, which is far away from the training region with $N < 178$. The predictive power of the ANN model is constrained when it is used to describe the region far from the training data set.

IV. SUMMARY

In this work, the ANN models with different inputs are built and trained to calculate nuclear α-decay half-lives. The physical features, which involve the angular momentum and deformation of parent nuclei, are used to improve the predictive ability of ANN model to describe α-decay half-lives. A total of 606 experimental α-decay half-lives are extracted to test the predictive ability of ANN model. When incorporating the angular momentum effect as an input in the ANN model, the corresponding root-mean-square deviation
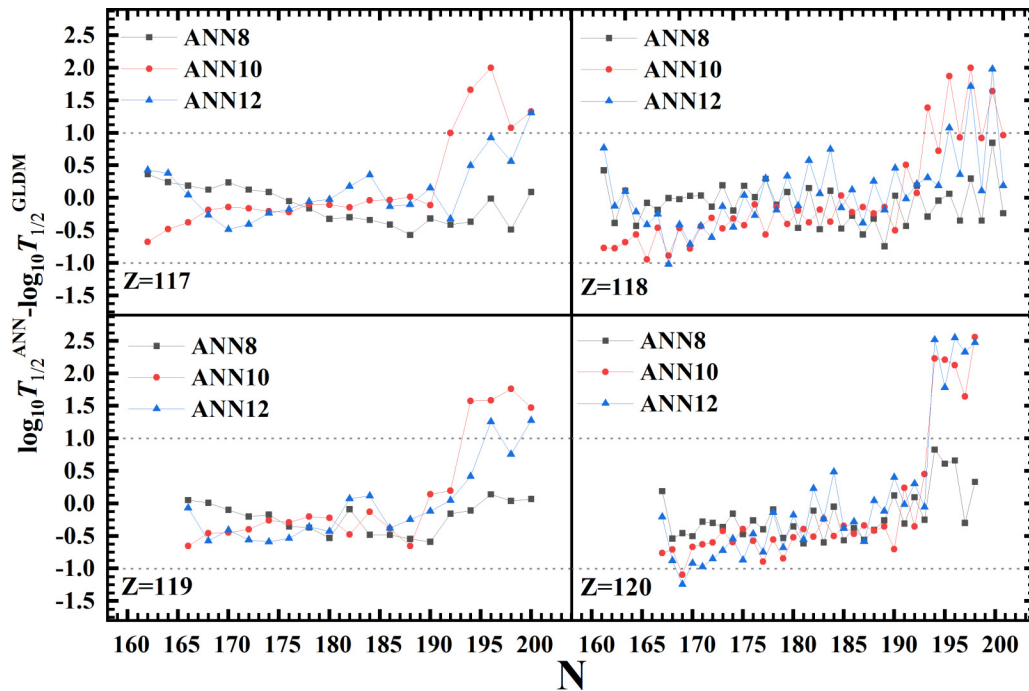
FIG. 7. Deviations between the various results from the ANN models and those from the GLDM model [50] for the α-decay half-lives of nuclei with $Z = 117$, 118, 119, and 120. The gray dashed lines represent the deviation of the decimal logarithms of $T_{1/2}^{ANN}/T_{1/2}^{GLDM}$ is within 1.

reduces from 0.581 to 0.335. Similarly, by incorporating the deformation effect as an input, the corresponding root-mean-square deviation reduces from 0.404 to 0.350. When both the angular momentum and deformation effects are considered, the ANN performs best with a root-mean-square deviation value of 0.334. It shows that the predictive power of α-decay half-lives can be improved when the angular momentum transferred by α particle and the quadrupole deformation of parent nuclei are considered in ANN models. Finally, ANN models are used to study α-decay half-lives in the superheavy nuclear region, where the experimental data are rare. The characteristics of the predicted α-decay half-lives imply that $N = 184$ could be the next neutron close shell beyond $N = 126$.

[1] G. Gamow, Z. Phys. **51**, 204 (1928).
[2] R. W. Gurney and E. U. Condon, Nature (London) **122**, 439 (1928).
[3] G. Royer, J. Phys. G **26**, 1149 (2000).
[4] G. Royer and B. Remaud, Nucl. Phys. A **444**, 477 (1985).
[5] G. Royer, Nucl. Phys. A **848**, 279 (2010).
[6] D. M. Joseph, N. Ashok, and A. Joseph, Eur. Phys. J. A **54**, 8 (2018).
[7] X. D. Sun, P. Guo, and X. H. Li, Phys. Rev. C **93**, 034316 (2016).
[8] J. G. Deng, J. C. Zhao, D. Xiang, and X. H. Li, Phys. Rev. C **96**, 024318 (2017).
[9] J. M. Dong, W. Zuo, J. Z. Gu, Y. Z. Wang, and B. B. Peng, Phys. Rev. C **81**, 064309 (2010).
[10] C. Xu and Z. Z. Ren, Phys. Rev. C **74**, 014304 (2006).
[11] V. E. Viola and G. T. Seaborg, J. Inorg. Nucl. Chem. **28**, 741 (1966).
[12] Y. J. Ren and Z. Z. Ren, Phys. Rev. C **85**, 044608 (2012).
[13] B. A. Brown, Phys. Rev. C **46**, 811 (1992).

[14] C. Qi, F. R. Xu, R. J. Liotta, and R. Wyss, Phys. Rev. Lett. **103**, 072501 (2009).
[15] A. Boehnlein, M. Diefenthaler, N. Sato, M. Schram, V. Ziegler, C. Fanelli, M. Hjorth-Jensen, T. Horn, M. P. Kuchera, D. Lee, W. Nazarewicz, P. Ostroumov, K. Orginos, A. Poon, X.-N. Wang, A. Scheinker, M. S. Smith, and L.-G. Pang, Rev. Mod. Phys. **94**, 031003 (2022).
[16] W. B. He, Q. F. Li, Y. G. Ma, Z. M. Niu, J. C. Pei, and Y. X. Zhang, Sci. China Phys. Mech. Astron. **66**, 282001 (2023).
[17] Z. M. Niu, H. Z. Liang, B. H. Sun, W. H. Long, and Y. F. Niu, Phys. Rev. C **99**, 064307 (2019).
[18] T. Bayram, S. Akkoyun, and S. O. Kara, Ann. Nucl. Energy **63**, 172 (2014).
[19] R. Utama, W.-C. Chen, and J. Piekarewicz, J. Phys. G, Nucl. Part. Phys **43**, 114002 (2016).
[20] S. Akkoyun, T. Bayram, S. O. Kara, and A. Sinan, J. Phys. G: Nucl. Part. Phys. **40**, 055106 (2013).
[21] L. Neufcourt, Y. Cao, W. Nazarewicz, and F. Viens, Phys. Rev. C **98**, 034318 (2018).

[22] Z. M. Niu and H. Z. Liang, Phys. Lett. B **778**, 48 (2018).

[23] Z. M. Niu, J. Y. Fang, and Y. F. Niu, Phys. Rev. C **100**, 054311 (2019).

[24] Z. M. Niu and H. Z. Liang, Phys. Rev. C **106**, L021303 (2022).

[25] U. B. Rodrguez, C. Z. Vargas, M. G. Gonçalves, S. D. Barbosa, and F. Guzman, J. Phys. G **46**, 115109 (2019).

[26] H. Q. You, Z. Z. Qu, R. H. Wu, H. Z. Su, and X. T. He, Symmetry **14**, 1006 (2022).

[27] Q. F. Song, L. Zhu, and J. Su, Chin. Phys. C **46**, 074108 (2022).

[28] T. X. Huang, X. H. Wu, and P. W. Zhao, Commun. Theor. Phys. **74**, 095302 (2022).

[29] F. P. Li, Y. J. Wang, Z. P. Gao, P. C. Li, H. L. Lü, Q. F. Li, C. Y. Tsang, and M. B. Tsang, Phys. Rev. C **104**, 034608 (2021).

[30] X. Zhang, X. Liu, Y. Huang, W. Lin, H. Zheng, R. Wada, A. Bonasera, Z. Chen, L. Chen, J. Han, R. Han, M. Huang, Q. Hu, Q. Leng, C. W. Ma, G. Qu, P. Ren, G. Tian, Z. Xu, Z. Yang *et al.*, Phys. Rev. C **105**, 034611 (2022).

[31] L. Yang, C. J. Lin, Y. X. Zhang, P. W. Wen, H. M. Jia, D. X. Wang, N. R. Ma, F. Yang, F. P. Zhong, S. H. Zhong, and T. P. Luo, Phys. Lett. B **807**, 135540 (2020).

[32] Y. D. Song, R. Wang, Y. G. Ma, X. G. Deng, and H. L. Liu, Phys. Lett. B **814**, 136084 (2021).

[33] M. O. Kuttan, J. Steinheimer, K. Zhou, and H. Stoecker, Phys. Rev. Lett. **131**, 202303 (2023).

[34] W.-J. Xie and B.-A. Li, Astrophys. J **899**, 4 (2020).

[35] M. P. Kuchera, R. Ramanujan, J. Z. Taylor, R. R. Strauss, D. Bazin, J. Bradt, and R. Chen, Nucl. Instrum. Methods Phys. Res. Sect. A **940**, 156 (2019).

[36] S. L. Chen, T. X. Wang, Z. Zhang, R. F. Li, S. Yuan, R. Y. Zhang, C. X. Yuan, C. Y. Zhang, and J. Y. Zhu, Phys. Rev. Appl. **19**, 034028 (2023).

[37] T. Li, Y. Chen, S. B. Wang, K. Han, H. Lin, K. X. Ni, and W. Wang, J. High. Engergy Phys. 05 (2023) 200.

[38] G. Saxena, P. K. Sharma, and P. Saxena, J. Phys. G: Nucl. Part. Phys. **48**, 055103 (2021).

[39] C. Q. Li, C. N. Tong, H. J. Du, and L. G. Pang, Phys. Rev. C **105**, 064306 (2022).

[40] R. H. Stuewer, Gamow's theory of alpha-decay, in *The Kaleidoscope of Science: The Israel Colloquium: Studies in History, Philosophy, and Sociology of Science Volume 1*, edited by E. Ullmann-Margalit (Springer Netherlands, Dordrecht, 1986), pp. 147–186.

[41] M. Riedmiller, Comput. Stand. Interfaces **16**, 265 (1994).

[42] M. W. Kirson, Nucl. Phys. A **798**, 29 (2008).

[43] R. F. Casten and N. V. Zamfir, J. Phys. G: Nucl. Part. Phys. **22**, 1521 (1996).

[44] R. F. Casten, D. S. Brenner, and P. E. Haustein, Phys. Rev. Lett. **58**, 658 (1987).

[45] A. E. Lovell, A. T. Mohan, T. M. Sprouse, and M. R. Mumpower, Phys. Rev. C **106**, 014305 (2022).

[46] X. X. Dong, R. An, J. X. Lu, and L. S. Geng, Phys. Rev. C **105**, 014308 (2022).

[47] G. Audi, F. G. Kondev, M. Wang, W. J. Huang, and S. Naimi, Chin. Phys. C **41**, 030001 (2017).

[48] M. Wang, G. Audi, F. Kondev, W. J. Huang, S. Naimi, and X. Xu, Chin. Phys. C **41**, 030003 (2017).

[49] W. J. Huang, G. Audi, M. Kondev, F. Kondev, S. Naimi, and X. Xu, Chin. Phys. C **41**, 030002 (2017).

[50] J. G. Deng, H. F. Zhang, and G. Royer, Phys. Rev. C **101**, 034307 (2020).

[51] Z. Y. Wang, Z. M. Niu, Q. Liu, and J. Y. Guo, J. Phys. G: Nucl. Part. Phys. **42**, 055112 (2015).

[52] V. Y. Denisov and A. A. Khudenko, Phys. Rev. C **79**, 054614 (2009).

[53] M. Ismail, A. Y. Ellithi, M. M. Botros, and A. Abdurrahman, Phys. Rev. C **86**, 044317 (2012).

[54] M. Ismail, W. M. Seif, A. Adel, and A. Abdurrahman, Nucl. Phys. A **958**, 202 (2017).

[55] S. H. Cheng, Z. S. Ge, L. G. Cao, and F. S. Zhang, J. Phys. G: Nucl. Part. Phys. **48**, 095106 (2021).

[56] D. S. Delion, A. Sandulescu, and W. Greiner, Phys. Rev. C **69**, 044318 (2004).

[57] P. Möller, J. Nix, W. Myers, and W. Swiatecki, At. Data Nucl. Data Tables **59**, 185 (1995).

[58] A. Sobiczewski, F. Gareev, and B. Kalinkin, Phys. Lett. **22**, 500 (1966).

[59] A. Staszczak, A. Baran, and W. Nazarewicz, Phys. Rev. C **87**, 024320 (2013).

[60] N. Wang and M. Liu, Phys. Rev. C **84**, 051303(R) (2011).

[61] A. Sobiczewski, Phys. Rev. C **94**, 051302(R) (2016).

[62] J. G. Deng, J. C. Zhao, P. C. Chu, and X. H. Li, Chin. Phys. C **41**, 124109 (2017).

[63] J. G. Deng, J. C. Zhao, P. C. Chu, and X. H. Li, Chin. Phys. C **42**, 044102 (2018).

[64] https://t2.lanl.gov/nis/data/astro/molnix96/spidat.html.